UAV-based Smart Rock Positioning for Determination of Bridge Scour Depth

H.B. Zhang [1,2], Z.C. Li [1], A. Reven [1], B. Scharfenberg [1], G. Chen [1], J.P. Ou [2]

[1] *Missouri University of Science and Technology – U.S., Email:* zhanghaib@mst.edu
[2] *Harbin Institute of Technology (Shenzhen) – China*

Abstract

This study aims to predict the depth of scour hole developed around a bridge pier with one smart rock. A 3-axis magnetometer was assembled on an unmanned aerial vehicle (UAV) to measure magnetic fields before and after the smart rock has been deployed as the UAV flew around the bridge pier. A 3-axis high resolution GPS unit was fixed on the UAV to ensure accurate measurements of the latitude, longitude and altitude of the magnetometer. The GPS and the magnetometer measurements were synchronized to output the coordinate and magnetic field intensity correspondingly. A simple optimization algorithm was used to predict the position of the smart rock with an accuracy of less than 0.5 m. In addition, a lab test was performed to understand the effect of UAV motors on the intensity of magnetic field. The test results demonstrated that the UAV motors had negligible influence on the magnetic intensity measured at a distance of over 0.75 m. The UAV-based rock positioning method was compared favorably with the traditional crane-based rock positioning method in multiple field tests.

1. Introduction

Scour and other hydraulic induced failures accounted for 58% of all bridge failures (Lagasse *et al.*, 1997), resulting in direct loss of lives and hundreds of millions of dollars in damage repair. For instance, 10 people lost their lives during the collapse of the I-90 Bridge over the Schoharie Creek in New York in 1987 when a footing foundation was inadequately protected from the formation of a scour hole that undermined the pier (NTSB, 1988). The cost of flood repairs during the 1980s was estimated to be $300 million (Butch, 1996). Between 1993 and 1995, the costs for the Midwest floods, Georgia and Virginia were $178 million, $130 million, and $40 million, respectively (Mueller, 2000). Additionally, bridge collapses due to scour can have a dramatic impact on local communities with financial impact estimated to be five times the actual repair cost (Rhodes and Trent, 1993). Therefore, it is necessary to protect these critical infrastructure elements against scour-induced potential damage.

Scour induced damage can be prevented by armoring the riverbed around bridge piers to reduce the amount of scour or by modifying the river hydraulics to reduce the peak flow, both requiring a significant amount of time and financial resources for implementation. Scour monitoring, however, can be implemented quickly at a reduced cost relative to other preventive measures. For this reason, Highway Engineering Circular (HEC) No.23 considers scour

monitoring as a viable countermeasure for scour critical bridges (Lagasse *et al.*, 2009).

The existing monitoring methods, however, cannot be applied to assess the condition of bridge scour in real-time because the continuous change in river and flow conditions required for the prediction of the maximum scour depth (Ali and Karim, 2002, Salaheldin *et al.*, 2004) is not made available during a flood event. Real-time monitoring and assessment of bridge scour is critical not only to maintaining ground transportation services but also ensuring the transportation safety in hours or days during flood events (NTSB, 1988). Therefore, real-time field scour monitoring is crucial for a more accurate prediction of scour and a further calibration of bridge design equations.

Smart rocks proved to have the potential for real-time scour monitoring (Chen *et al.*, 2018), which will automatically roll down the bottom of their surrounding scour hole under strong current as a diver would find a critical scour condition. The magnetometer measures magnetic fields surrounding the smart rocks. The position of the magnetometer can be accurately determined using a total station. The difference in two measurements over time thus represents the movement of the smart rocks during that time period. The vertical movement represents the development of scour depth over time. The traditional method used a crane to hold the monitoring device to locate the smart rock (Chen *et al.*, 2016), which often requires the closure of a lane of traffic and is time-consuming in data collection.

This paper proposed an unmanned aerial vehicle (UAV)-based smart rock positioning system for the determination of bridge scour depth. Through remote sensing, a magnetometer and GPS units installed on a UAV can relate the maximum scour depth to the engineer in charge. This critical data is used by engineers to assess the stability of foundations due to scour hazards.
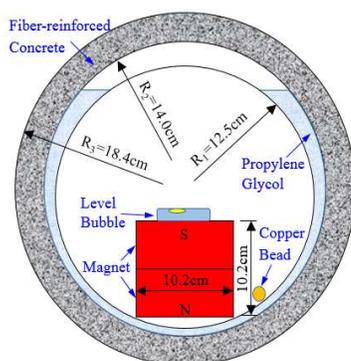
2. Fabrication of Smart Rock

Figure 1 Schematic view of smart rock

Figure 2 Fabricated smart rock and its deployment

A smart rock is schematically shown in Figure 1. The smart rock consists of a fiber-reinforced concrete shell encasement, inside and outside organic glass balls, low viscosity liquid propylene glycol filled in between two balls, two cylindrical N42 magnets, a level indicator, and some copper beads distributed as balanced weights. The diameters of inside and outside balls are 12.5 cm and 14.0 cm, respectively. The magnet is 10.2 cm in diameter and 5.1 cm in height, which is

fixed on the inside ball with glue. The magnet is designed to remain in equilibrium and be free to rotate once the inside ball floats within the outside ball. Therefore, the central axis of the magnet is perpendicular to the ground and the south pole of the magnet is directly upward based on unbalanced weights. The diameter of the smart rock is 18.4 cm with a density of 1495 kg/m^3. One fabricated smart rock is shown in Figure 2 when ready for installation. The design of smart rocks was based on the critical velocity of water flow (Chen *et al.*, 2016).

3. Localization Algorithm

As shown in Figure 3, the XYZ Cartesian coordinate system is selected such that the geomagnetic field vector, B_E, is parallel to the XOY plane. The direction of the geomagnetic field depends on whether the investigated site is located in north or south hemisphere of the Earth. Since the project (bridge) sites in this study are located in North America, the geomagnetic field vector slightly points to the geographical North and faces to the ground with a corresponding dip angle of the field site, θ. Therefore, the Earth's magnetic field vector is B_E = (-$B_E \cos\theta$, -$B_E \sin\theta$, 0)^T in the global coordinate system. The magnitude of B_E is measured by means of the magnetometer prior to deployment of the magnet at a project site. The magnetic field vector of the magnet, B_m, can be calculated by using Eq. (1):
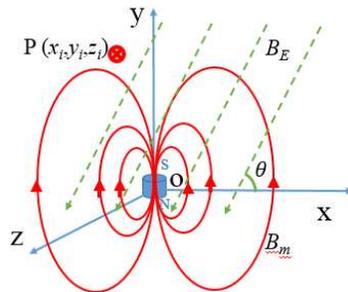

Figure 3 The magnetic field at an arbitrary point

$$
\begin{cases}
B_{mxi} = k \dfrac{3x_i y_i}{r_i^5} \\[2mm]
B_{myi} = k \dfrac{2y_i^2 - x_i^2 - z_i^2}{r_i^5} \\[2mm]
B_{mzi} = k \dfrac{3z_i y_i}{r_i^5}
\end{cases}
\tag{1}
$$

where $r_i = \sqrt{x_i^2 + y_i^2 + z_i^2}$, and k is the coefficient related to magnetic property of the magnet.

Given the coefficients k and θ and the Earth's magnetic intensity B_E for the project site, the total magnetic intensity of the Earth and the magnet, B_{Ti}, at any point P (x_i, y_i, z_i) is a function of (x_i, y_i, z_i) only. It can be expressed into:

$$
B_{Ti} = \sqrt{(B_{mxi} - B_E \cos\theta)^2 + (B_{myi} - B_E \sin\theta)^2 + (B_{mzi})^2}
\tag{2}
$$

To determine the location (3 parameters) of a magnet, measurements must be taken at a minimum of three stations in practical applications. Eq. (2) is a high-order nonlinear function of 3 location parameters. To solve the parameters (x_i, y_i, z_i), the sequential quadratic programming (SQP) algorithm (Boggs and Tolle, 1989) was used to iteratively find the optimization solution

for the position of the magnet from the high-order nonlinear equation sets. The algorithm was implemented in MATLAB through the use of Fmincon code for non-linearly constrained optimization problems.

4. The Effect of UAV on the Magnetic Field

The significant advantages of measuring the magnetic field with UAV are no traffic control requirement, no need for a heavy test crane, and no time-consuming test process. However, the rotation of UAV motors generates current and may thus influence the measurement of magnetic field. There are 8 motors in a UAV. One of the motors was used to test for potential interference on the magnetic field measurement. Figure 4 shows the test setup of a motor and a magnetometer. When the motor turns on, the current of the motor can be monitored by the Dynamometer (Model 1580). The magnetic field is measured by the magnetometer that is set at various distances from 0.25 m to 1 m in 0.25 m increment. The Z axis along the magnetometer sensor head points to the motor. The test results are presented in Figure 4. It can be clearly seen from Figure 4 that the motor-induced current has negligible effect on the magnetic field at a measurement distance of over 0.75 m. Since this distance is 0.92 m when the magnetometer is assembled on a UAV as shown in Figure 5, the motor effect is neglected. Note that the UAV itself is mainly made of non-ferrous materials.
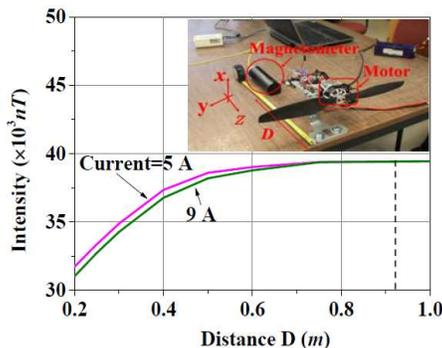

Figure 4 Change in magnetic field intensity with measurement distance under various applied currents
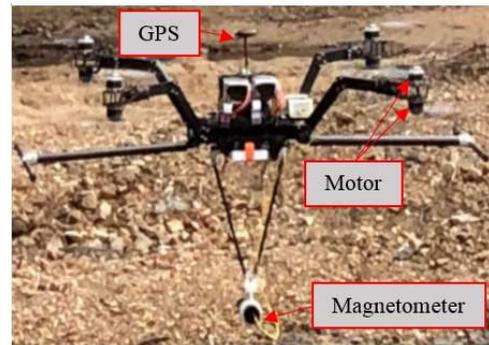

Figure 5 UAV installed with a magnetometer and a GPS unit

5. Field Tests

The I-44W Roubidoux Creek Bridge (No. L0039) in Waynesville, MO, was used as the first test site to verify the validity of smart rock positioning with a UAV. The bridge is a ten-span, steel-girder structure to support two lanes of westbound traffic on Interstate 44. As shown in Figure 6, Pier 7 is located in the main channel of the river. The downstream side of Pier 7 is scour critical. A series of field tests were performed in different seasons after flooding to validate the localization algorithm and understand the accumulated movement of a smart rock between flood events or during normal water flow.

5.1 Test setup

A smart rock was deployed near Pier 7, which would automatically roll into the bottom of a

scour hole when formed with unknown location and depth as deposits around the hole are washed away. Before and after the smart rock was deployed, the magnetic field and corresponding coordinate data were collected simultaneously by the magnetometer and GPS unit installed on the UAV that is controlled by a pilot to fly above the water, as shown in Figure 7. The data was transmitted wirelessly to the monitoring station. This setup allows for the rapid collection of a dense array of field intensity data at bridge sites. The large data set will improve the accuracy of smart rock localization and movement prediction.

Figure 6 The I-44W Roubidoux Creek Bridge

Figure 7 Smart rock positioning through UAV

5.2 Test results

To verify the localization algorithm and monitoring method, the calculated coordinates of the smart rock obtained from the traditional crane- and the UAV-based method were individually compared with the ground truth position measured using a total station. As shown in Table 1, the monitoring error between two monitoring methods is basically the same, indicating the reliability of the UAV-based method. The errors of two field tests using the UAV-based method are less than 0.36 m. The movement during five field tests was displayed on a three-dimensional contour map of the riverbed.

Table 1 Comparison of different monitoring methods

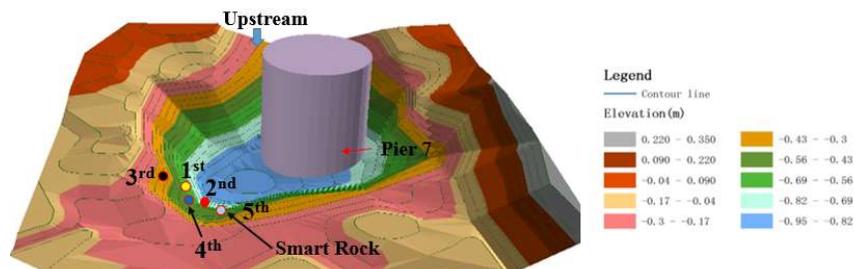| Monitoring method	Date	Calculated coordinate			Measured coordinate			Error
		X	Y	Z	X	Y	Z	
CRANE (1st)	11/06/2015	0.06	23.49	-3.03	0.09	23.24	-3.04	0.26
CRANE (2nd)	04/14/2016	0.55	24.38	-3.21	0.37	24.60	-3.38	0.33
CRANE (3rd)	10/20/2016	0.00	22.73	-2.59	0.00	22.63	-2.87	0.30
UAV (4th)	01/24/2018	0.02	23.50	-2.89	0.25	23.77	-2.93	0.36
UAV (5th)	05/10/2018	0.49	25.00	-2.81	0.45	24.78	-3.01	0.30

Figure 8 Movement of the smart rock during five field tests

6. Conclusions

In this paper, a UAV-based smart rock positioning system was proposed for the determination of bridge scour depth. A 3-axis magnetometer and a GPS unit were installed on the UAV for magnetic field and coordinate measurements simultaneously. The effect of the UAV on the magnetic field was found negligible when the magnetometer was placed at a distance of 0.75 m from the nearest UAV motor. The UAV-based positioning method was compared well with the traditional crane-based positioning method. Both methods resulted in less than 0.36 m in rock positioning error.

References

Ali, K. H. and Karim, O. (2002). "Simulation of flow around piers." *J. Hydra. Res.*, 40(2), pp. 161-174.

Boggs, P. and Tolle, J. (1989). "A Strategy for Global Convergence in a Sequential Quadratic Programming Algorithm." *SIAM J. Numer. Ana.*, 26(3), pp. 600-623.

Butch, G. K. (1996). "Evaluation of selected instruments for monitoring scour at bridges in New York." *North American Water and Environment Congress& Destructive Water*, ASCE.

Chen, G. D., Tang, Y., Chen, Z. C., Guo, C. R., Bao, Y., Fan, L. T., Hu, X. Y., Klegseth, M. and Li, Z. C. (2016). *Smart Rock Technology for Real-time Monitoring of Bridge Scour and Riprap Effectiveness – Design Guidelines and Visualization Tools*. US Department of Transportation. Report No. OASRTRS-14-H-MST.

Chen, Y. Z., Tang, F. J., Li, Z. C., Chen, G. D. and Tang, Y. (2018). "Bridge scour monitoring using smart rocks based on magnetic field interference." *Smart Mater. Struct.*, 27(8), pp. 085012.

Lagasse, P. F., Clopper, P. E., Pagán-Ortiz, J. E., Zevenbergen, L. W., Arneson, L. A., Schall, J. D. and Girard, L. G. (2009). "Bridge scour and stream instability countermeasures: experience, selection, and design guidance." *Hydra. Eng. Circular*. I(23), FHWA NHI HEC-23.

Lagasse, P. F., Richardson, E. V., Schall, J. D. and Price, G. R. (1997). *Instrumentation for measuring scour at bridge piers and abutments*. NCHRP Report 396: TRB, National Research Council, Washington, D. C.

Mueller, D. S. (2000). "National Bridge Scour Program - measuring scour of the streambed at highway bridges." *U.S. Geological Survey*, Reston, VA.

NTSB (1988). Collapse of New York Thruway (I-90) Bridge, Schoharie Creek, near Amsterdam, New York, April 5, 1987. Washington, D. C., National Transportation Safety Board. NTSB Number: HAR-88/02, NTIS Number: PB88-916202.

Rhodes, J. and Trent, R. (1993). "Economics of floods, scour, and bridge failures." *Proceedings of the National Conference of Hydraulic Engineers*. San Francisco, California, ASCE.

Salaheldin, T. M., Imran, J. and Chaudhry, M. H. (2004). "Numerical modeling of three-dimensional flow field around circular piers." *J. Hydra. Eng.*, 130(2), pp. 91-100.